Kersevan *EPJ Techniques and Instrumentation* (2022) 9:12
https://doi.org/10.1140/epjti/s40485-022-00087-w

EPJ Techniques and Instrumentation

RESEARCH ARTICLE Open Access

The FCC-ee vacuum system, from conceptual to prototyping

Roberto Kersevan[1*]

*Correspondence:
roberto.kersevan@cern.ch
[1]Vacuum Surfaces and Coatings Group, Technology Department, CERN, Geneva, Switzerland

Abstract

The FCC-ee is a very challenging accelerator project from the point of view of vacuum. Apart from the sheer size of the machine, a twin-ring of 100 km circumference, the vacuum system design must be capable of dealing with the low-energy 45.6 GeV, high-current version of the machine (the *Z*-pole) as well as the higher energy, lower current versions. The main difficulty is related to the very much different synchrotron radiation (SR) spectra of the *Z*-pole vs the other energies, in particular the ttbar at 182.5 GeV. The critical energy of the SR spectrum of the *Z*-pole is 19.5 keV, while the ttbar exceeds 1.2 MeV. It is particularly challenging in terms of shielding the beryllium chamber in the detectors, for the Machine Detector Interface (MDI) area. We discuss the evolution of the vacuum system design for the arc sections, and some new ideas on NEG-coating, SR absorbers, and pumping system, with the aim to build prototypes soon, in the framework of the FCC Innovation Study program. The design of the vacuum hardware depends on the choices made for the magnets, and the required shielding from high-energy radiation generated by the circulating beam interacting with the residual gas and the interaction of the intense SR fans with the photon. There is also an important collaboration with the engineering integration of the vacuum system in the tunnel, particularly considering the full-energy booster injector, which is not detailed here. We also briefly describe the raytracing montecarlo modelling efforts carried out in the MDI area, and its pumping configuration.

Keywords: Vacuum; Pumping system; Montecarlo simulations; Synchrotron radiation; e– e+ colliders; Higgs factories

1 Machine parameters relevant to vacuum

Since the publication of the FCC Conceptual Design Report [1], the layout of the FCC tunnels and access shafts have changed considerably, namely a shorter ring circumference to avoid some geological limitations has been established [2]. Throughout this paper we will refer to the machine size and geometry of ref. [1], as many numerical simulations have been carried out on it, and in the end the changes would not affect the vacuum environment that much. See Fig. 1 and Table 1 in [1], partly reproduced here.

For electron or positron storage rings, if vacuum is concerned, the main machine parameters of interest are beam energy, current, bending radius, linear and areal synchrotron radiation (SR) power densities and photon flux. They determine, via the photon-stimulated

Table 1 Machine and vacuum-relevant parameters (IP: interaction point)

	Z	W	*H*	$t\bar{t}$	
Circumference (km)			97.756		
Bending radius (km)			10.760		
Free length to IP *l** (m)			2.2		
Solenoid field at IP (T)			2.0		
Full crossing angle at IP θ (mrad)			30		
SR power/beam (MW)			50		
Beam energy (GeV)	45.6	80	120	175	182.5
Beam current (mA)	1390	147	29	6.4	5.4

Table 2 Critical energy vs beam energy and cut-off fractions for flux and power

E (GeV)	E_c (keV)	k_f
45.6	19.55	0.9280
80	105.54	0.9592
120	356.20	0.9730
175	1104.75	0.9816
182.5	1252.96	0.9824

desorption (PSD) mechanism, the amount of gas given off during operation with stored beams, Q. The formula relating the PSD gas load to beam energy E (GeV) and current I (mA) for SR fan generated by a magnet with local dipole radius ρ (m) is

$$Q = \eta(\text{mol/ph}) \cdot F(\text{ph/s}) \cdot k, \tag{1}$$

where k converts from (mol/s) to (mbar · l/s) via the ideal gas equation $PV = nRT$.

At 20°C (hereafter called "room temperature", RT) $k = 4.047 \cdot 10^{-20}$ mbar · l/mol.

The photon flux F is given in practical units by $F = 8.08 \cdot 10^{17} E(\text{GeV}) \cdot I(\text{mA}) \cdot k_F$, where k_F is a factor accounting for the fraction of the photon flux spectrum above the threshold of 4 eV. This threshold (cut-off) is chosen in most vacuum studies because it is well known that PSD is mediated by the emission of photoelectrons (PE), and for most vacuum chamber materials used in accelerators there is no PE generation below 4 eV. The k_F factors are shown on Table 2.

The photon flux F must also be considered to evaluate the electron-cloud (EC) effect, which must be minimized as much as possible [1, 3].

The SR power is given by the formula $P(\text{W}) = 88.46 \cdot I(\text{mA}) \cdot E^4(\text{GeV})/\rho(\text{m}) \cdot k_P$, where k_P is a factor similar to k_F but accounting for the fraction of SR power generated above the 4 eV cut-off. k_P is very close to 1, except when SR is generated by weaker fringe fields or quadrupoles.

Another important parameter is the SR critical energy, given in practical units by

$$\epsilon_c(\text{keV}) = 2.218 \cdot E^3(\text{GeV})/\rho(\text{m}) \tag{2}$$

Given the dependence on the cube of the beam energy, the critical energy varies by a factor of 64 between the low-energy Z and the high-energy tt.

The design of the FCC-ee must cope with the very much different spectra during the 15 years long program (see Fig. 4 in [1]), starting at the Z and bringing the machine to its design parameters in a rather short time, of the order of 2 years. The Z is characterized

by the largest photon flux, and therefore related PSD gas load, and it is therefore the most challenging machine to design. In addition, given its sheer size, the twin ring machine must be designed in such a way to adapt to all the future beam energy increases, from 45.6 to 182.5 GeV.

2 Synchrotron radiation spectra

The SR photon flux spectra for the 5 beam energies are shown on Fig. 1.

In the inset, the linear photon flux generated along each meter of dipole orbit at the nominal current is indicated, and the critical energy as well.

Starting with the W energy the fraction of photon flux generated above 100 keV, which is the Compton edge for aluminium becomes large. Table 3 shows the fraction of such photons, for each beam energy.

This has important effects on the number of molecules which are generated inside the vacuum chamber, and their geometrical distribution, as the Compton-scattered electrons and photons in the bulk of the vacuum chamber material (and surrounding magnets) may go back to the vacuum chamber and generate a cascade of lower-energy photons and PEs and related PSD effects.

This had been noticed during the beam energy increase of the Phase-2 of the LEP machine [4] and it is also predicted by FLUKA calculations [5]. It is one of the reasons why the last dipoles before the interaction points have a weaker field to keep the critical energy of the SR generated along them below 100 keV, see Sect. 9 below.

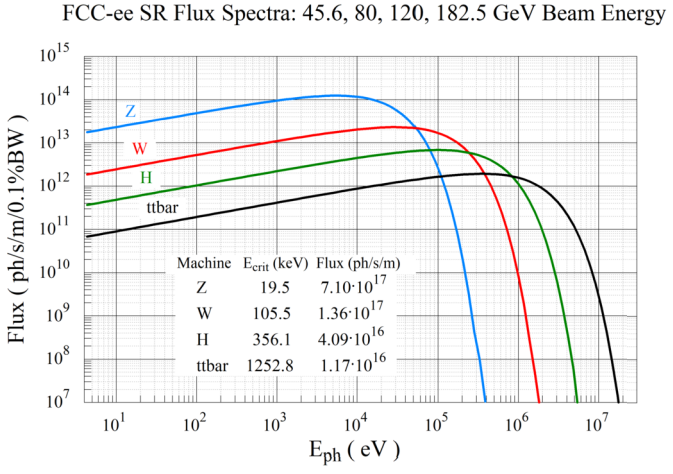

Figure 1 SR photon flux at nominal currents

Table 3 Percent of SR photon flux generated above 100 keV

E (GeV)	% Flux > 100 keV	B (mT)
45.6	0.064	14.1
80	9.22	27.7
120	28.85	37.1
175	47.81	54.1
182.5	49.72	56.5

3 Choice of materials

The vacuum chamber material of choice must have a good compromise between mechanical, thermal, and electrical properties, and material procurement and fabrication costs. Extruded aluminium has some advantages compared to copper but unfortunately it is very transparent to high energy SR photons, which would lead to detrimental effects in terms of irradiation of tunnel components [5].

OFS-grade copper alloy has been chosen, as it is a material which has well known welding/brazing properties, good mechanical and thermal characteristics, and very good electrical conductivity.

The pumping domes, see Sect. 5, are made of 316 LN sheets and machined parts. A different copper alloy could be used to make the flanges, see Sect. 6. Bellows are made of stainless steel, with hydroformed convolutions welded to forged 316 LN stainless steel parts. RF contact fingers are made of BeCu C17410 material, a well-tested solution: their optimized geometry and placement, though, will be the subject of future tests. A permanent radiation-hard cold-sprayed bake-out system using ceramic plasma coating techniques and metallic cold-spray coating is proposed and will be tested by the CERN vacuum group [6]. For the SR absorbers, see Sect. 5, the material will be copper alloy. What technology will be used to join them to the vacuum chambers will be determined by prototyping and testing, they have to withstand a very large surface power density at the tt energy, due to the extremely small vertical divergence of the SR fan, less than 3 microradians above and below the plane of the orbit contain 95% of the SR dipole power [7].

4 Gas loads

An estimate of the PSD gas load can be obtained using Eq. (1) and the linear photon flux F' (in ph/s/m) shown on the inset of Fig. 1, assuming an average PSD molecular yield of 10^{-6} mol/ph, a value which is usually obtained after an integrated beam dose close to 1000 A · h [8]. Q' is the corresponding linear gas load density in mbar · l/s/m.

Clearly, the energies above the Z will profit from the pre-conditioning at the very large photon flux of the Z, except for any new chambers which will be installed during energy upgrades. This may be the case for the areas in the long straight sections, as many RF cavities will have to be installed to account for the SR energy loss and reduce the energy sawtooth effect which would be detrimental for the experiments [9]. Along the arcs there will be no need to replace the vacuum chambers as the energy of the beams will be increased.

For the different machines, the linear outgassing yields Q' are shown on Table 4.

Here we assume that there will be no noticeable additional gas load coming from effects such as the electron cloud (EC). EC studies for existing machines [3] show that there are mitigation measures that can be taken against it, such as amorphous carbon coating, surface texturing (e.g. laser ablation techniques), and more, see Sect. 10.

Table 4 Linear PSD outgassing yields

E (GeV)	Q' (mbar · l/s/m)
45.6	$2.90 \cdot 10^{-8}$
80	$5.58 \cdot 10^{-9}$
120	$1.67 \cdot 10^{-9}$
175	$5.40 \cdot 10^{-10}$
182.5	$4.78 \cdot 10^{-10}$

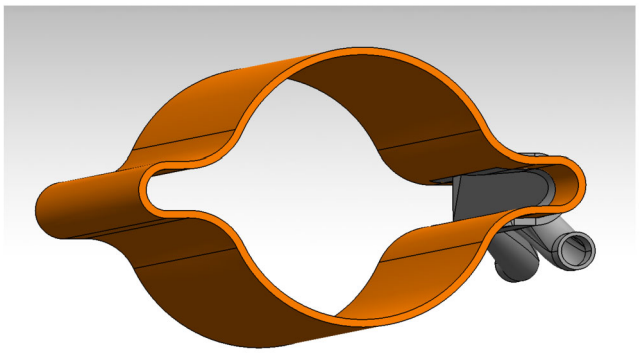

Figure 2 Vacuum chamber cross section with one SR absorber. The circular part is 70 mm internal diameter and the horizontal width in the plane of the orbit is 115 mm

5 Vacuum chamber geometry

The cross-section of the chamber fits all the arc magnets' pole design [10, 11]. It implements the SuperKEKB concept, a circular tube with two "winglets" in the plane of the orbit. The circle has an internal diameter of 70 mm, compared to the 90 mm of SuperKEKB [7, 8]. The chamber cross section can be extruded, avoiding longitudinal welds, with a slightly larger thickness in the area of the winglets to help relieve an area of high mechanical stress due to chamber forming [6]. Discrete photon absorbers are placed at a variable distance to intercept all the primary SR fan from the arc dipoles and quadrupoles [7]. Figure 2 illustrates the concept, with one SR absorber having an inclined surface to reduce the SR power density to manageable levels [7], around 40 W/mm^2 for the Z energy machine, with an absorber inclination of 45°. A vertical absorber would receive a power density higher by a factor of 1.4. Preliminary calculations, not detailed here, show that it would be advisable to remain near 40 W/mm^2, on considerations of the temperature of the copper at the cooling channels.

6 Pumping system

NEG-coating has been chosen as the main pumping mechanism, mainly because it guarantees low PSD yield and low secondary electron yield (SEY) as well. Additional pumping for non-getterable gases is given by lumped pumps. NEG-coating is a mature technology, with more than 20 years of implementation on lepton machines with high PSD effects [12]. Additional pumping is obtained by installing lumped pumps, either NEG or ion-pumps, near some of the SR absorbers along the arcs [7, 11]. Their exact type, number, and location is yet to be determined, and a cost-benefit analysis will have to be carried out.

7 Montecarlo simulations

Extensive modelling using raytracing montecarlo codes SYNRAD+ and Molflow+ has been carried out. Both codes can import the vacuum chamber geometry models from CAD programs. SYNRAD+ calculates the SR fan in the dipole approximation, i.e. no interference effects, using the orbits imported from lattice codes such as MADX. It then generates a mapping of the SR irradiation on all surfaces, which can be converted into PSD gas desorption at a chosen time (beam dose), using Eq. (1) Molflow+ imports the SYNRAD+ file and runs the molecular flow simulation [13].

8 Arcs

We have modelled both rings with and without SR absorbers: the conditioning time with absorbers is shorter than that without because the absorbers concentrate on a short length, typically 150 mm, the SR flux that would otherwise hit 5.6 m on average along the arcs. It is well documented in literature the fact that PSD outgassing rate Q'' (in mbar $\cdot$ l/s/cm^2) scales as a power function of the accumulated SR photon flux density F'' (in ph/s/cm^2), like $Q'' \approx A \cdot F''^{-\alpha}$, where α is typically $0.5 < \alpha < 0.8$ [14], and A is a unit conversion factor. Concentrating the SR photon flux density by a factor of between 35 and 40 (depending on the location along the arc), the conditioning time shortens by an average factor of 8.5 with respect to the case when the photon flux is distributed along the external side of the chamber, like LEP did. This speed up is important as it allows a faster conditioning of the machine at the Z energy, as mentioned at the end of Sect. 1. The advantage of implementing NEG-coating along all chambers has been demonstrated too [7, 11].

9 Machine Detector Interface (MDI) area

Combined raytracing montecarlo simulations have been carried out for the MDI regions as well. A new design of the interaction region chamber, which now removes the need for high-order-mode-absorbing ferrites has been implemented in SYNRAD+, and then in Molflow+, calculating the number of photons reaching the beryllium chamber, and their spectra [15]. The last 600 m upstream of the interaction point (IP) are equipped with SR photon absorbers on both sides of the vacuum chamber, due to the anti-bending in that area, in order to decrease the photon flux scattered towards the IP. Lumped NEG pumps are located near some of these absorbers, and a low average pressure can be obtained (in the low 10^{-10} mbar range), so that the interaction of the incoming stored beam and the residual gas can be minimised (bremsstrahlung). FLUKA simulations having these pressure profiles as input for the gas distribution are under development now [16], first for the arc and then for the MDI region as well.

10 Future work

The design of many vacuum components such as vacuum chamber extrusion, SR absorbers, low-loss, low-impedance RF contact fingers with rectangular bellows, shape-memory alloy-based oval flanges, pumping ports, beam-position monitor blocks is underway: prototypes will be fabricated and tested during the remainder of the FCC IS study program.

We plan to test the vacuum chamber and photon absorbers behaviour using SR at the BESTEX beamline at the KARA light source [17], on 2 m-long prototypes. As BESTEX is not capable to reproduce the high SR power density of FCC-ee the SR absorbers will need to be tested from the point of view of their thermal behaviour using an appropriate source, e.g., an electron beam device.

Preliminary design of bellows assemblies with RF contact fingers has also been carried out, see Fig. 3.

A thermo-mechanical analysis of the behaviour of the SR absorbers has been carried out, to determine the position and number the cooling holes in the body of the absorbers [19].

Prototypes of shape memory alloy (SMA)– based vacuum flanges are also being developed [18], as shown on Fig. 4.

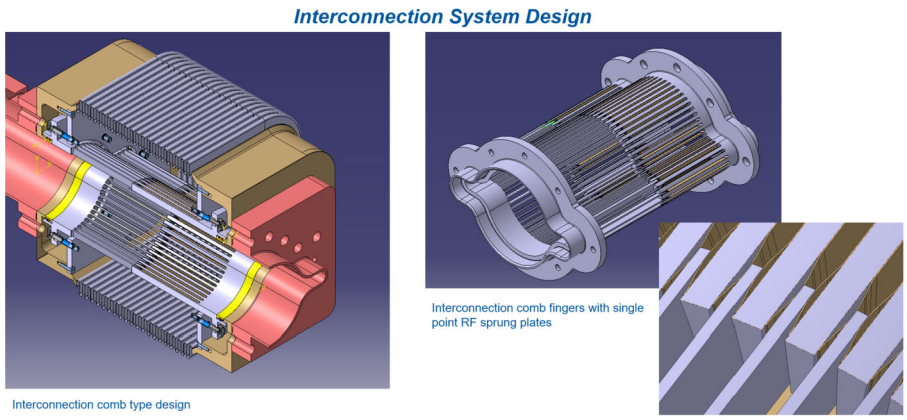

Figure 3 Interconnection comb-type RF finger design, with details

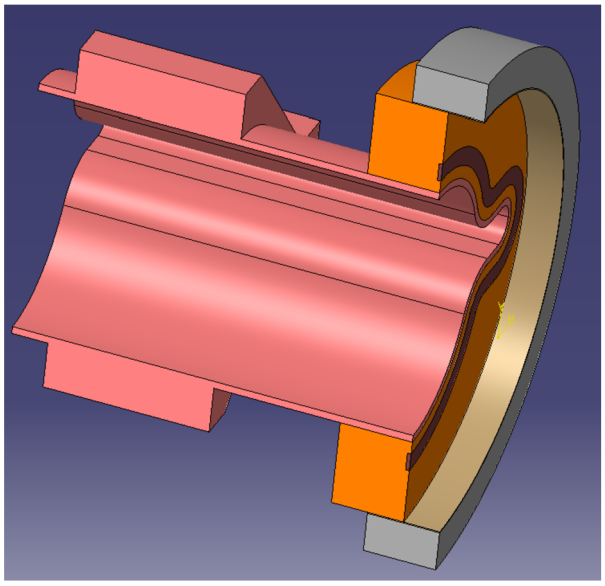

Figure 4 Concept of a SMA-based vacuum flange, with integrated additive manufacturing beam-position block (on the left, 4× BPM buttons at 45° not drawn)

We have also identified the ideal length of the arc vacuum chambers compatible with the design of the magnets, to minimize the number of flanges: 12 meters seems to be feasible also in terms of NEG-coating deposition, which would be carried out in a horizontal position by applying new technology developed for the HL-LHC program at CERN [20]. Prototyping of this configuration will be carried out as soon as chambers will be available. There is also a parallel activity of building a test section of the arc, approximatively 25 m long, simulating the tunnel environment, so that tunnel integrations studies can be carried out on mock-ups.

Acknowledgements
The author wishes to thank his colleagues F. Santangelo and S. Rorison for providing Figs. 2, 4 and 3; M. Morrone and C. Garion for fruitful discussions, thermal calculations, and mechanical design guidelines; M. Ady for paper editing and reviewing the manuscript.

Funding
This research was funded by FCCIS – The Future Circular Collider Innovation Study. This INFRADEV Research and Innovation Action project receives funding from the European Union's H2020 Framework Programme under grant agreement no. 951754.

Abbreviations
FCC, Future Circular Collider; MDI, Machine Detector Interface; SR, Synchrotron Radiation; PSD, Photon Stimulated Desorption; EC, Electron Cloud; PE, Photoelectrons; OFS, Oxygen-free; RF, Radiofrequency; SEY, Secondary Electron yield; NEG, Non-evaporable getter; IP, interaction point; SMA, shape memory alloy.

Availability of data and materials
Data available upon request from the author. The montecarlo simulation codes Molflow+ and SYNRAD+ are available for download from https://molflow.web.cern.ch.

Declarations

Ethics approval and consent to participate
Not applicable.

Consent for publication
The author declares that he has obtained the consent from his institution to publish the article.

Competing interests
The author declares no competing interests.

Author contribution
RK was the sole contributor to all sections of the paper. The author read and approved the final manuscript.

Publisher's Note

Received: 29 August 2022 Accepted: 2 November 2022 Published online: 18 November 2022

References

1. Benedikt M, Blondel A, Brunner O, Capeans Garrido M, Cerutti F, Gutleber J, Janot P, Jimenez JM, Mertens V, Milanese A, Oide K, Osborne JA, Otto T, Papaphilippou Y, Poole J, Tavian LJ, Zimmermann F. FCC-ee: the lepton collider: future circular collider conceptual design report volume 2. Future circular collider. Technical report. CERN, Geneva; 2018. https://doi.org/10.1140/epjst/e2019-900045-4. https://cds.cern.ch/record/2651299.
2. Gutleber J. FCC baseline V1.0 and fallback scenarios. 144th FCC-ee Optics Design Meeting. & 15th FCCIS WP2.2 Meeting. https://indico.cern.ch/event/1065778/.
3. Yaman F, Iadarola G, Kersevan R, Ogur S, Ohmi K, Zimmermann F, Zobov M. Mitigation of electron cloud effects in the fcc-ee collider. Technical report, CERN. 2022. https://cds.cern.ch/record/2804867.
4. Gröbner O. Experience from the LEP vacuum system. In: Workshop on VLHC. 2001. www.capp.iit.edu/workshops/epem/Transparencies/Grobner.pdf.
5. Cerutti F. Impact of SR in lepton collider arcs. In: FCC study kick-off meeting. Geneva. 2014. https://indico.cern.ch/event/282344/contributions/1630742/.
6. Garion C. CERN, personal communication.
7. Kersevan R. FCC-ee beam vacuum challenges, concepts and future R&D plans. In: FCC week. 2019. https://indico.cern.ch/event/995850/contributions/3449896/.
8. Suetsugu Y. Experience with the vacuum system of SuperKEKB. In: FCC week. 2021. https://indico.cern.ch/event/995850/contributions/4426079/.
9. Wenninger J. FCC-ee CM energy: impact of the RF system. In: FCC-ee polarization workshop. 2017. https://indico.cern.ch/event/669194/.
10. Bauche J. Design of the FCC-ee collider magnets. In: FCC week. 2021. https://indico.cern.ch/event/995850/timetable/.
11. Kersevan R. Arc vacuum system and synchrotron radiation. In: FCC week. 2021. https://indico.cern.ch/event/995850/contributions/4404304/.
12. Costa Pinto P. History and potential of Non-Evaporable Getter (NEG) technology. Workshop on Advanced Materials and Surfaces. Geneva: CERN. https://indico.cern.ch/event/229108/.
13. Ady M, Kersevan R. Recent developments of Monte-Carlo codes MolFlow+ and SynRad+. 10th Int. Particle Accelerator Conf. Melbourne, Australia. https://doi.org/10.18429/JACoW-IPAC2019-TUPMP037.
14. Malyshev O. Beam induced desorption. In: CERN accelerator school vacuum for particle accelerators. Glumslöv, Sweden. 2017. https://indico.cern.ch/event/565314/timetable/.
15. Kersevan R. Synchrotron radiation simulations in the IR. FCC-ee MDI meeting #34 and FCCIS WP2.3 meeting #5. https://indico.cern.ch/event/1071912/.

16. Humann B. Synchrotron radiation studies for the FCC-ee arc with FLUKA. In: FCC week. 2021. https://indico.cern.ch/event/995850/contributions/4405383/.
17. Gonzalez LA et al. Commissioning of a beam screen test bench experiment with a future circular hadron collider type synchrotron radiation beam. Phys Rev Accel Beams. 2019;22:083201. https://journals.aps.org/prab/pdf/10.1103/PhysRevAccelBeams.22.083201.
18. Niccoli F et al. NiTi shape memory alloy pipe couplers for ultrahigh vacuum systems: development and implementation. Smart Mater Struct. 2022;31:065014.
19. Morrone M. Preliminary thermo-mechanical analysis of the FCC-ee. Unpublished internal CERN technical note, available upon request.
20. Costa Pinto P. In-situ amorphous carbon coating of the beam screen of LHC's standalone magnets. In: Proceedings of the 11th international particle accelerator conference IPAC'20. Caen, France. 2020.